Chemical Papers (2020) 74:591–599
https://doi.org/10.1007/s11696-019-00899-3

ORIGINAL PAPER

An asymmetric supercapacitor based on $NiCo_2O_4$ nanosheets as anode and partially reduced graphene oxides/carbon nanotubes as cathode

Ke Yan[1] · Juan Wu[1] · Ying-Ying Wang[1] · Ning-Ning Liu[1] · Ji-Tao Li[2] · Yong-Ping Gao[3] · Zhi-Qiang Hou[1]

Received: 31 January 2019 / Accepted: 9 August 2019 / Published online: 19 August 2019

Abstract

Nickel–cobalt oxide has been given more attention to being used as the supercapacitor's electrode materials due to its two-dimensional layered structure, good electron conductivity, and excellent stability. In this work, $NiCo_2O_4$ nanosheets were successfully prepared by the simple solvothermal reaction and the thermal treatment process. Under the three-electrode system, it exhibits a maximum specific capacitance of 978 F/g at 1.5 A/g and good cycle stability. Meanwhile, a freestanding of partially reduced graphene oxides/carbon nanotubes (PRGO/CNTs) film was obtained by the vacuum filter and solvothermal methods, which can provide a wide potential window of − 1 ~ 0 V and a maximum specific capacitance of 236 F/g at 0.5 A/g. Finally, an asymmetric supercapacitor of PRGO/CNTs//$NiCo_2O_4$ was assembled, which exhibits good electrochemical performance, such as specific capacitance of 82 F/g at 0.5 A/g, energy density of 18.8 Wh/kg at 0.32 kW/kg, and 99.5% of capacitance retention after 5000 cycles at 5 A/g. This test results reveal that PRGO/CNTs//$NiCo_2O_4$ ASC has great potential for practical application in energy storage systems.

Keywords $NiCo_2O_4$ nanosheets · PRGO/CNTs · Specific capacitance · Supercapacitor

Introduction

Recently, supercapacitors are regarded as novel energy storage systems, which have attracted considerable interest due to its high-energy density, rapid charge and discharge, and excellent cycle life. Based on these merits, supercapacitors have an important application value in hybrid vehicles, flash cameras, and backup power, etc. To meet the people's demand, scientists devote much time and energy to understanding its charge storage and conversion mechanism, further developing the advanced supercapacitor devices (Bidhan et al. 2017; Hou et al. 2017; Hou et al. 2018a, b; Ma et al. 2019; Pai and Kalra 2018; Pai et al. 2018; Thakur and Lokhande 2019; Xiong et al. 2018; Xing et al. 2018). Currently, people have realized that excellent electrode materials and a rational supercapacitor structure are the key factors on which supercapacitor's electrochemical performance depends.

Until now, carbon materials [graphene (Ma et al. 2015), carbon nanotube (Wang et al. 2018a, b), carbon fiber (Mao et al. 2018), and active carbon (Liu et al. 2019)], transition metal oxides/hydroxides [MnO_2 (Zhao et al. 2019), V_2O_5 (Pandit et al. 2017a, b), $NiCo_2O_4$ (Wang et al. 2018a, b), $NiFe_2O_4$ (Zhang et al. 2019), $Ni(OH)_2$ (Syed et al. 2017), and FeO(OH) (Thakur and Lokhande 2018)], transition metal sulfide [MoS_2 (Mohit et al. 2018), NiS (Guan et al. 2017), and FeS_2 (Sandhya et al. 2018) etc.], transition carbides (Yuan et al. 2018), and conductive polymers [poly(3,4-ethylenedioxythiophene)-poly(styrenesulfonate) (Luo et al. 2018), polyaniline (Zhou et al. 2018), and polypyrrole (Huang et al. 2018; Zhi and Zhou 2018)] have been investigated as supercapacitor's electrode materials. All of the binary transition metal oxides have shown some advantages of good electron conductivity, superior capacitance, good performance rate, and excellent stability (Ma et al. 2016), which is better than that of carbon materials, single metal oxides/hydroxides, transition metal sulfides,

✉ Zhi-Qiang Hou
hou_zq@sina.cn

[1] College of Chemistry and Chemical Engineering, Zhou Kou Normal University, Henan 466001, People's Republic of China

[2] College of Physics and Telecommunication Engineering, Zhou Kou Normal University, Henan 466001, People's Republic of China

[3] College of Science and Technology, Xinyang College, Xinyang 464000, People's Republic of China

transition carbides and conductive polymers. For instance, carbon materials have low specific capacitance; single metal oxides/hydroxides have bad electron conductivity, low rate performances, and a short cycle life; the morphology of transition metal sulfides is hard to control; transition carbides are prepared through harsh chemical reactions; and conductive polymers have bad rate capability and cycle life due to its kinetic's irreversible. In view of this, binary transition metal oxides are considered as ideal electrode materials for supercapacitors.

Herein, $Ni(NO_3)_2{\cdot}6H_2O$ and $Co(NO_3)_2{\cdot}6H_2O$ are employed to synthesize NiCo–OH nanosheets by the simple solvothermal reaction, then NiCo–OH nanosheets are further heated at 300 °C for 2 h to obtain $NiCo_2O_4$ nanosheets. The as-prepared $NiCo_2O_4$ nanosheets could provide high electron conductivity, enough reactive sites, and high specific surface area, which are favorable to obtain a good electrochemical performance. Next, the positive electrode of $NiCo_2O_4$ is prepared based on $NiCo_2O_4$, black carbon, and PTFE. Then, the electrochemical properties of $NiCo_2O_4$ electrode were investigated in 6 M KOH electrolyte. And the test results exhibit an ideal specific capacitance of 978 F/g, good rate capability, and good cycle life (98.5% capacitance retention after 3000 cycles). Furthermore, PRGO/CNTs were prepared via vacuum filter and solvothermal methods, as negative electrode materials. And the PRGO/CNTs electrode shows specific capacitance of 236 F/g at 0.5 A/g in 6 M KOH electrolyte. Finally, we used $NiCo_2O_4$ electrode as positive electrode, PRGO/CNTs as negative electrode, and 6 M KOH electrolyte to build an asymmetric supercapacitor of PRGO/CNTs//$NiCo_2O_4$. Similarly, the electrochemical properties of PRGO/CNTs//$NiCo_2O_4$ were also evaluated, which exhibited maximum specific capacitance of 82 F/g, maximum energy density of 18.8 Wh/kg, and 99.5% specific capacitance retention after 5000 cycles. This indicates that $NiCo_2O_4$ electrode could be regarded as an ideal electrode material and an asymmetric supercapacitor of PRGO/CNTs//$NiCo_2O_4$ also exhibits good electrochemical behavior.

Experimental section

Preparation of $NiCo_2O_4$ nanosheets as a positive material

Desired reagents $Ni(NO_3)_2{\cdot}6H_2O$, $Co(NO_3)_2{\cdot}6H_2O$ and hexamethylenetetramine were dissolved in 30 mL methanol solution, then the mixture solution was transferred to 50 mL reactor equipment heated at 180 °C for 12 h (Ma et al. 2016). Next, NiCo–OH was obtained after washing with purified water and ethanol several times. Finally, NiCo–OH was heated at 300 °C for 2 h to obtain $NiCo_2O_4$ nanosheets.

Preparation of PRGO/CNTs as a negative material

First, the mass ratio of GO and CNTs is controlled at 9:1. After the mixture dispersion liquid was treated by the ultrasonic operation, the GO/CNTs film is obtained by the vacuum method (Yang et al. 2019). We bend the GO/CNTs film, and put it into a metal tube (height: 4.5 cm, out diameter: 1.8 cm, and inner diameter: 1.7 cm). Then, the metal tube with GO/CNTs film and 30 mL ethanol were transferred into the 50 mL reactor equipment, further heating at 150 °C for 6 h to obtain the PRGO/CNTs films.

Electrochemical tests

For the positive electrode, 75% of $NiCo_2O_4$ nanosheets, 15% of carbon black, and 5% of PTFE were adequately mixed to form a uniform mixture. And the mixture was rolled to obtain a thin film, which was then heated at 120 °C for 12 h to remove redundant water. The cut film was pressed onto between two pieces of nickel foam at 10 MPa to obtain a positive electrode. For the negative electrode, the PRGO/CNTs electrode is obtained as well as the positive electrode. All the electrochemical tests were conducted using the electrochemical working station CHI 660E system at room temperature. And the Hg/HgO electrode, Pt plate, and 6 M KOH solution were used as reference electrode, counter electrode, and electrolyte, respectively. Each electrode was tested in the three-electrode system. And the PRGO/CNTs//$NiCo_2O_4$ was tested in the two-electrode systems. The electrochemical tests mainly included cyclic voltammetry (CV), galvanostatic charge–discharge (GCD), rate capability, impedance, and cycling life.

Characterization

Information about electrode materials regarding phase structure, compose, morphology, specific surface area and pore size distribution was identified using X-ray diffraction (XRD), inductively coupled plasma mass spectrometry (ICP-MS), field emission scanning electron microscopy (FESEM), transmission electron microscopy (TEM), high-resolution transmission electron spectroscopy (HR-TEM), and Brunauer–Emmett–Teller (BET) method.

Results and discussion

To seek for a high electrochemical performance of supercapacitor device, we prepared the $NiCo_2O_4$ nanosheets via the simple solvothermal method and thermal treatment process. And the $NiCo_2O_4$ nanosheets were characterized by XRD,

ICP-MS, SEM, TEM, HR-TEM, BET, and electrochemical tests to understand its structure, morphology, specific surface area, and electrochemical behaviors. Then, a freestanding of PRGO/CNTs film was prepared by vacuum filter and solvothermal reduced methods and it was also characterized by XRD, SEM, TEM, BET, and electrochemical tests. Finally, an asymmetric supercapacitor is assembled based on $NiCo_2O_4$ nanosheets, PRGO/CNTs film, nickel foam, and 6 M KOH electrolyte. The electrochemical performance of asymmetric supercapacitor was investigated to evaluate its application value. The details are given in the following.

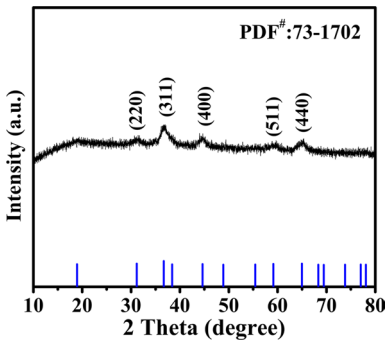

Fig. 1 XRD patterns of $NiCo_2O_4$ nanosheets

$NiCo_2O_4$ nanosheets as a positive electrode

The as-prepared samples were characterized by XRD to certify their phase structure, as shown in Fig. 1. From Fig. 1, it is observed that there are five diffraction peaks at 31.2°, 36.7°, 44.6°, 59.1°, and 65.0° assigned to the (220), (331), (400), (510), and (440) crystal phases of $NiCo_2O_4$ (PDF card: 73-1702). And these diffraction peaks are weak and broad, suggesting poor crystallinity. Furthermore, ICP-MS is used to further ensure the atomic ratio of Ni/Co. The test results indicate that the atomic ratio of Ni/Co is 1:1.78, and it means that the atomic ratio of Ni/Co is approximate to 1:2 in the as-prepared samples. Overall, it reveals that the as-prepared samples are composed of $NiCo_2O_4$ powers.

The morphological characterization of $NiCo_2O_4$ powers was investigated using SEM, TEM and HR-TEM to examine its morphology information. As shown in Fig. 2a, the morphology of $NiCo_2O_4$ powers was first examined by SEM to further certify the element types of the samples via the EDS mapping method. From Fig. 2b–d, it is easily

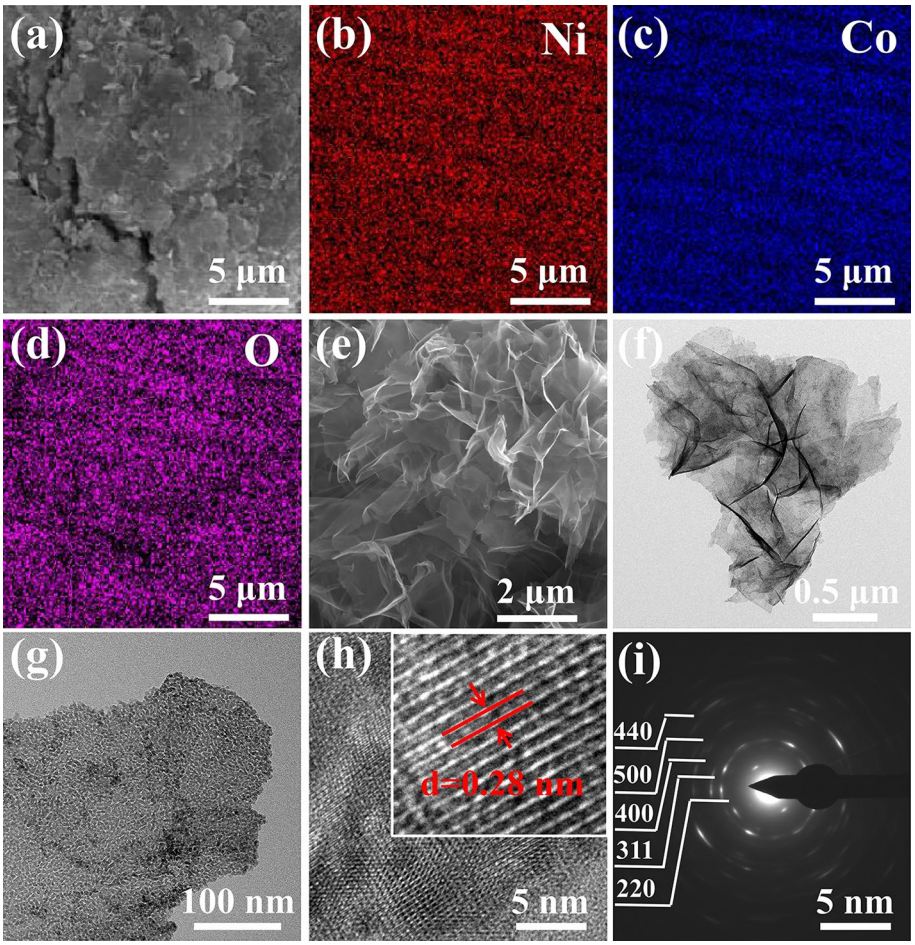

Fig. 2 **a** SEM images of $NiCo_2O_4$ nanosheets; **b–d** EDS mapping of Ni, Co, and O elements, respectively; **e** SEM images of $NiCo_2O_4$ nanosheets; **f**, **g** TEM images of $NiCo_2O_4$ nanosheets; **h** HR-TEM image of $NiCo_2O_4$ nanosheets; **i** SAED pattern of $NiCo_2O_4$ nanosheets

observed that the as-prepared samples comprise Ni, Co, and O elements, which is in conformity with the XRD analytical results. And the Ni, Co, and O elements are uniformly distributed in the samples. Figure 2e clearly exhibits that the morphology of as-prepared samples is wrinkled laminar nanosheets. Figure 2f further shows that the $NiCo_2O_4$ nanosheets take on a graphene-like structure. A magnified view of $NiCo_2O_4$ nanosheets (Fig. 2g) clearly indicates the ultrathin nanosheets. To certify the samples of crystal lattice spacing, $NiCo_2O_4$ nanosheets were characterized by HR-TEM. The HR-TEM images (Fig. 2h) show visible lattice fringes with inter-planar space of 0.28 nm, assigning to (220) planes of the spinel $NiCo_2O_4$. Furthermore, selected area electron diffraction (SAED) patterns of the as-prepared samples are also conducted, as shown in Fig. 2i. The diffraction rings indicate poor crystallinity, and the diffraction pattern can be indexed to (220), (331), (400), (510), and (440) crystal phases of the spinel $NiCo_2O_4$, which is in conformity with XRD pattern.

Additionally, the specific surface area and pore size distribution of $NiCo_2O_4$ nanosheets are analyzed using BET methods by the adsorption and desorption of N_2. As shown in Fig. 3a, the nitrogen adsorption/desorption isotherms of $NiCo_2O_4$ nanosheets are typical II curves, revealing a small pore or mesoporous structure. And the BET-specific surface area of $NiCo_2O_4$ nanosheets is 119.15 m^2/g, with total pore volume of 0.118 cm^3/g. Figure 3b gives the pore size distribution of $NiCo_2O_4$ nanosheets. It is observed that $NiCo_2O_4$ nanosheets contain small pores (0–2 nm), mesopores (2–50 nm) and macropores (50–100 nm). And $NiCo_2O_4$ nanosheets exist in very small pores and mesopores. It suggests that the high specific surface area and very small pores/mesopores structure of $NiCo_2O_4$ nanosheets could provide good electrochemical performance.

After a series of XRD, ICP-MS, SEM, TEM, HR-TEM, and BET characterization, the electrochemical performance of $NiCo_2O_4$ nanosheets electrode was investigated in the three-electrode system, including cyclic voltammetry (CV), galvanostatic charge–discharge (GCD), rate capability, and cycle life, as shown in Fig. 4. In Fig. 4a, the CV tests are conducted at various sweet rates of 2, 4, 6, 8, and 10 mV/s in a suitable potential window of 0–0.5 V. The high current density value obtained at these scan rates could even reach 24 A/g at 10 mV/s, revealing high specific capacitance. CV curves exhibit two pairs of oxidation–reduction peaks at sweet rates of 2–6 mV/s, which are attributed to the following redox reactions (Hu et al. 2011): $NiCo_2O_4 + OH^- + H_2O \leftrightarrow NiOOH + 2CoOOH + 2e^-$, $CoOOH + OH^- \leftrightarrow CoO_2 + H_2O + e^-$. And CV curves take on one pair of oxidation–reduction peak at the sweet rates of 8–10 mV/s. And the area of CV curves gradually increases with the increasing current densities. Figure 4b shows that the GCD tests are performed at 0–0.48 V at the current densities of 1.5, 3, 4.5, 6, and 7.5 A/g. The charge and discharge time could reach 650 s at 1.5 A/g, revealing high specific capacitance. The specific capacitances of 978, 923, 894, 871, and 856 F/g were obtained at current densities of 1.5, 3, 4.5, 6, and 7.5 A/g, respectively (Fig. 4c). Meanwhile, $NiCo_2O_4$ nanosheets electrode also exhibits good rate capability, and 73.7% of specific capacitance is retained when the current densities vary from 1.5 A/g to 20 A/g. At last, the cycle stability of $NiCo_2O_4$ nanosheets is an important parameter to evaluate its practical application. So, the cycle stability is investigated, as shown in Fig. 4d. It could be observed that 98.5% of specific capacitance is kept after 3000 cycles at 15 A/g, suggesting good cycle stability. All of this revealed that the as-prepared $NiCo_2O_4$ nanosheets electrode has good electrochemical performance.

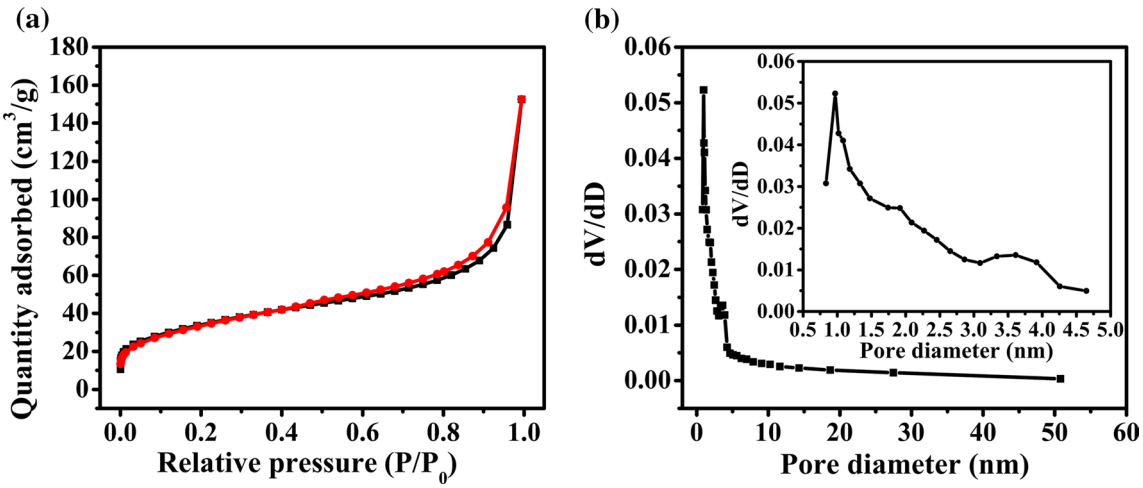

Fig. 3 Nitrogen adsorption/desorption isotherms (**a**) and pore diameter distribution (**b**) of the $NiCo_2O_4$ nanosheets

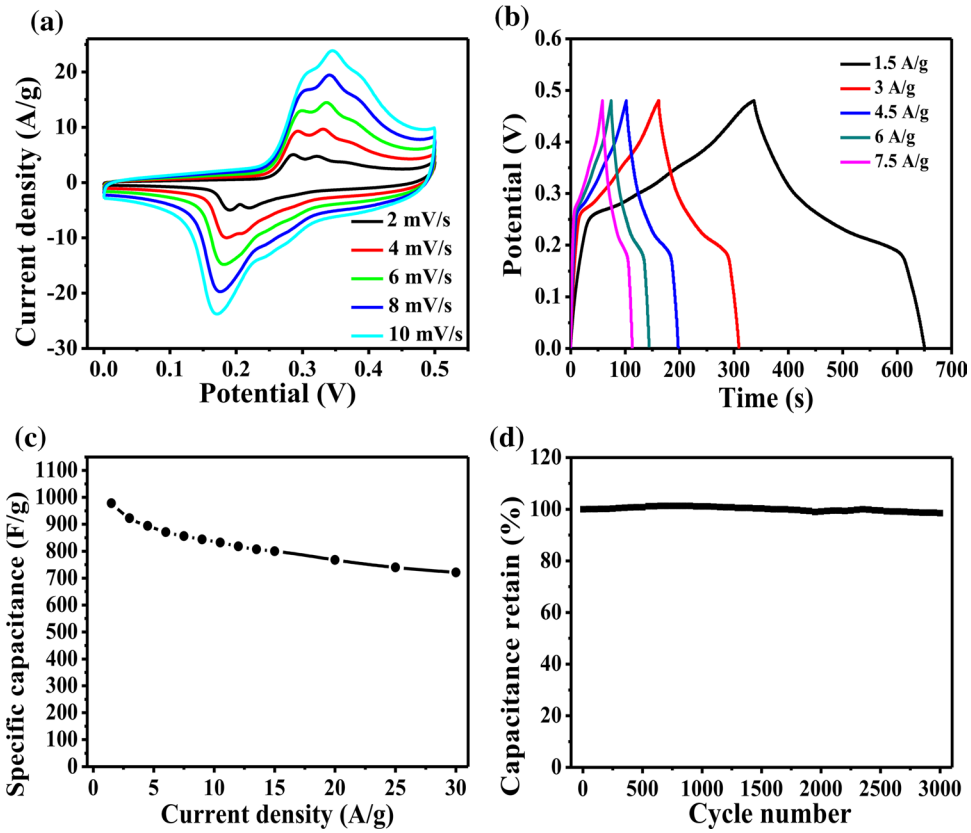

Fig. 4 **a** CV curves of $NiCo_2O_4$ nanosheets; **b** GCD curves of $NiCo_2O_4$ nanosheets; **c** specific capacitance versus current densities; **d** cycle life

PRGO/CNTs as a negative electrode

The information about phase structure and morphology of PRGO/CNTs were also attained using XRD, SEM, and TEM, as shown in Fig. 5. It is observed that the diffraction peaks of XRD spectra (Fig. 5a) mainly appear at 7.1°, 14.9° and 22.6°. Two diffraction peaks of 7.1° and 14.9° originate from GO. And the diffraction peak of 22.6° reveals the existence of graphene carbon. This indicates that the GO are only partially reduced in the solvothermal reaction procedure, which could enhance electrolyte infiltration to improve the electrochemical performance (Chen et al. 2013). From Fig. 5b, it is observed that the surface area of the samples take on a wave structure wrinkled by partially reduced graphene oxides and carbon nanotubes. After the PRGO/CNTs films is immersed in ethanol solvent, it is treated with high-power ultrasonic wave for several minutes to further characterize by TEM technology. TEM images of Fig. 5c, d show that the partially reduced graphene oxides strongly wrinkle with carbon nanotubes, suggesting a film with good flexible and mechanical strength.

Moreover, the specific surface area and pore size distribution of PRGO/CNTs films are also investigated using BET methods by the adsorption and desorption of N_2. In Fig. 6a, it is shown that the nitrogen adsorption/desorption isotherms of PRGO/CNTs films are typical

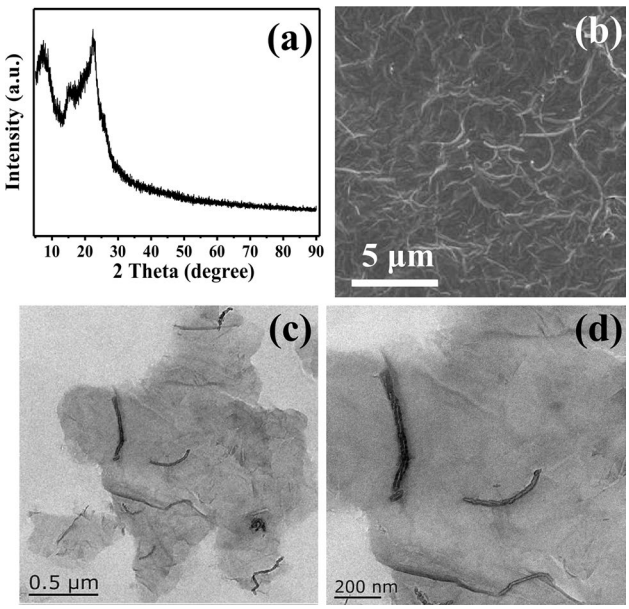

Fig. 5 **a** XRD patterns of PRGO/CNTs; **b** SEM images of PRGO/CNTs; **c**, **d** TEM images of PRGO/CNTs

IV curves. The BET-specific surface area of PRGO/CNTs films is 200.96 m^2/g, with total pore volume of 0.571 cm^3/g. The pore size distribution of PRGO/CNTs

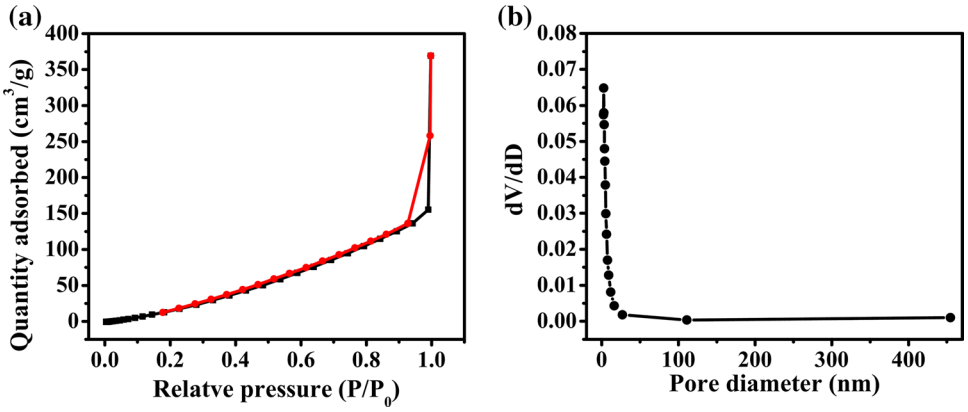

Fig. 6 Nitrogen adsorption/desorption isotherms (**a**) and pore diameter distribution (**b**) of PRGO/CNTs

films is exhibited in Fig. 6b. It is observed that PRGO/CNTs films contain many mesopores (2–50 nm) and few macropores (50–100 nm). Most of the mesopores are formed by thermal decomposition of GO in a 3D framework of GO/CNTs films. Based on the above mentioned, it is revealed that PRGO/CNTs films could provide the ideal specific capacitance.

Then, the electrochemical properties of PRGO/CNTs film are also measured by CV and GCD tests, as shown in Fig. 7. From Fig. 7a, the CV tests are performed at various scan rates of 10, 20, 30, 40, and 50 mV/s in a wide potential window of − 1 ~ 0 V. The shape of CV curves takes on a rectangle shape, revealing the charge storage provided by double capacitor. The area of CV curves also increases with the increasing current densities. Figure 7b depicts that all the GCD curves present an approximate triangle. The specific capacitances of 236, 200, 194, 182, 166, 162, and 161 F/g are obtained at the current densities of 0.5, 1, 2, 3, 4, and 5 A/g, respectively. In a word, the experimental results show that the PRGO/CNTs films as a negative materials could provide a wide potential window and an ideal specific capacitance.

Asymmetric supercapacitor PRGO/CNTs//$NiCo_2O_4$

Herein, an asymmetric supercapacitor of PRGO/CNTs//$NiCo_2O_4$ is assembled using Ni foam as collector, PRGO/CNTs films as negative material, $NiCo_2O_4$ as positive material, and 6 M KOH solution as electrolyte. And the CV, GCD, rate capability, impedance, and cycles are also tested to evaluate the electrochemical properties of PRGO/CNTs//$NiCo_2O_4$ ASC. After optimization, the suitable loading weight of positive materials and negative materials are 1.2 and 0.86 mg, respectively. The electrochemical tests of PRGO/CNTs//$NiCo_2O_4$ ASC are shown in Fig. 8. From Fig. 8a, it is observed that the potential window of this ASC is 1.3 V, because this potential window can avoid the polarization of the electrolytes. And CV curve's area for the PRGO/CNTs//$NiCo_2O_4$ ASC gradually increase with various scan rates of 10–50 mV/s. GCD curves of the PRGO/CNTs//$NiCo_2O_4$ ASC are shown in Fig. 8b, and the GCD tests are performed at the current densities of 0.5, 1, 2, 3, 4, and 5 A/g, respectively. The shape of these curves is a similar triangular wave, especially for GCD curves obtained under high current densities. In Fig. 8c, the specific capacitances are 82, 60, 49, 42, 37, and 34 F/g at the current densities of 0.5, 1, 2, 3, 4, and 5 A/g, respectively. In Fig. 8d, the EIS

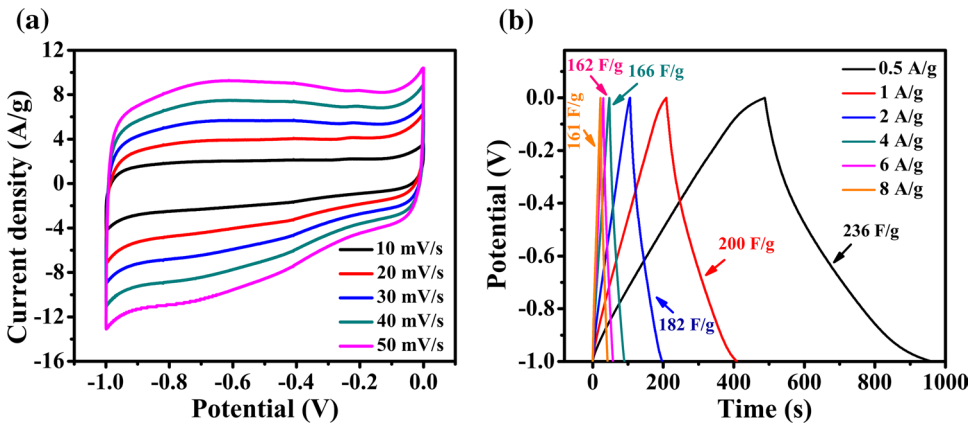

Fig. 7 **a** CV curves of PRGO/CNTs; **b** GCD curves of PRGO/CNTs

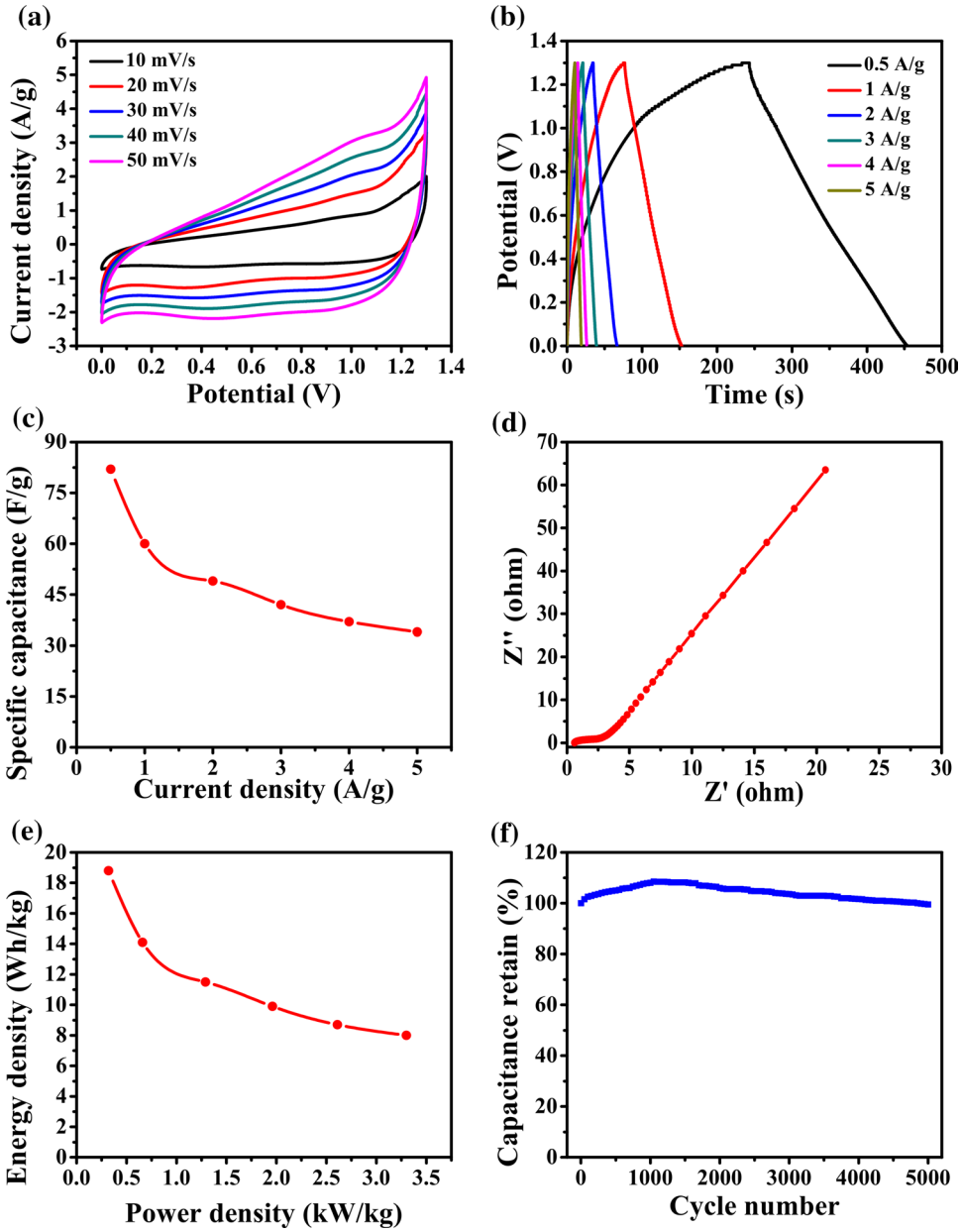

Fig. 8 **a** CV curves of PRGO/CNTs//$NiCo_2O_4$ ASC; **b** GCD curves of PRGO/CNTs//$NiCo_2O_4$ ASC; **c** specific capacitance versus current densities; **d** Nyquist plots; **e** Ragone plots of PRGO/CNTs//$NiCo_2O_4$ ASC; **f** cycle life

plots of PRGO/CNTs//$NiCo_2O_4$ ASC reveal its relative low intrinsic resistance. The Ragone plots of the PRGO/CNTs//$NiCo_2O_4$ ASC are depicted in Fig. 8e. The energy densities of PRGO/CNTs//$NiCo_2O_4$ ASC are 18.8, 14.1, 11.5, 9.9, 8.7, and 8.0 Wh/kg corresponding to the power densities of 0.32, 0.66, 1.29, 1.96, 2.61, and 3.30 kW/kg, respectively. The highest energy density of the PRGO/CNTs//$NiCo_2O_4$ ASC is more than that of the relative references, such as $Ni(OH)_2$/UGF//a-MEGO with a energy density of 13.4 Wh/kg at 65 W/kg (Ji et al. 2013), $CoMoO_4$//AC with a energy density of 14.5 Wh/kg at 18,000 W/kg (Yu et al. 2014), $Ni_{1.5}Co_{1.5}S_4$//RGO with a energy density of 17.7 Wh/kg at 23,250 W/kg (Chen et al. 2015), MoS_2 symmetric supercapacitor with a energy density of 18.43 Wh/kg at 1125 W/kg (Pazhamalai et al. 2019). Finally, the cycle stability of this asymmetric supercapacitor is investigated to evaluate its practical application, as shown in Fig. 8f. It is observed that 99.5% of capacitance retention is kept after 5000 cycles at a current density of 5 A/g, revealing its excellent cycle stability.

Conclusion

In this work, $NiCo_2O_4$ nanosheets are successfully prepared via a simple solvothermal route and thermal treatment process, which exhibit good electrochemical properties, such as high specific capacitance of 978 F/g and good cycle life.

Meanwhile, a freestanding of PRGO/CNTs film is obtained by vacuum filter and solvothermal reduced methods, which also possess good stability with maximum specific capacitance of 236 F/g at 0.5 A/g. And an asymmetric supercapacitor of PRGO/CNTs//$NiCo_2O_4$ was fabricated based on $NiCo_2O_4$ nanosheets as positive material, PRGO/CNTs film as negative material, and 6 M KOH solution as electrolyte. After optimization, PRGO/CNTs//$NiCo_2O_4$ ASC exhibits maximum specific capacitance of 82 F/g at 0.5 A/g, maximum energy density of 18.8 Wh/kg at 0.32 kW/kg, and excellent cycle stability. Based on the above mentioned, it could be seen that this PRGO/CNTs//$NiCo_2O_4$ ASC has great potential for practical application in energy storage systems.

Acknowledgements This work was supported by the National Natural Science Foundation of China (11604395), the Program for Science & Technology Innovation Talents in Universities of Henan Province (18HASTIT032), Innovation Fund of College of Chemistry and Chemical Engineering in Zhou Kou Normal University (HYDC201901, HYDC201904), High Level Personal Fund of Zhou Kou Normal University (ZKNUC2017043), Key Research Project of Henan Higher Education Institute (19A150045, 19A150052).

References

Bidhan P, Swapnil SK, Babasaheb RS (2017) Hexagonal VS_2 anchored MWCNTs: first approach to design flexible solid-state symmetric supercapacitor device. ACS Appl Mater Inter 9:44880–44891. https://doi.org/10.1021/acsami.7b13908

Chen LF, Huang ZH, Liang HW, Yao WT, Yu ZY, Yu SH (2013) Flexible all-solid-state high-power supercapacitor fabricated with nitrogen-doped carbon nanofiber electrode material derived from bacterial cellulose. Energy Environ Sci 6:3331–3338. https://doi.org/10.1039/c3ee42366b

Chen HC, Jiang JJ, Zhao YD, Zhang L, Guo DQ, Xia DD (2015) One-pot synthesis of porous nickel cobalt sulphides: tuning the composition for superior pseudocapacitance. J Mater Chem A 3:428–437. https://doi.org/10.1039/C4TA04420G

Guan B, Li Y, Yin BY, Liu KF, Wang DW, Zhang HH, Cheng CJ (2017) Synthesis of hierarchical NiS microflowers for high performance asymmetric supercapacitor. Chem Eng J 308:1165–1173. https://doi.org/10.1016/j.cej.2016.10.016

Hou ZQ, Wang ZY, Yang LX, Yang ZG (2017) Nitrogen-doped reduced graphene oxide intertwined with V_2O_3 nanoflakes as self-supported electrodes for flexible all-solid-state supercapacitors. RSC Adv 7:25732–25739. https://doi.org/10.1039/c7ra02899g

Hou ZQ, Tian FS, Gao YP, Wu W, Yang LX, Jia XL, Huang KJ (2018a) Nickel cobalt hydroxide/reduced graphene oxide/carbon nanotubes for high performance aqueous asymmetric supercapacitors. J Alloy Compd 753:525–531. https://doi.org/10.1016/j.jallcom.2018.04.245

Hou ZQ, Yang ZG, Gao YP (2018b) Synthesis of vanadium oxides nanosheets as anode material for asymmetric supercapacitor. Chem Pap 72:2849–2857. https://doi.org/10.1007/s11696-018-0504-9

Hu GX, Tang CH, Li CX, Li CX, Wang Y, Gong H (2011) The sol–gel-derived nickel-cobalt oxides with high supercapacitor performances. J Electrochem Soc 158:A695–A699. https://doi.org/10.1149/1.3574021

Huang LP, Rao WD, Fan LL, Xu J, Bai ZK, Xu WL, Bao HF (2018) Paper electrodes coated with partially-exfoliated graphite and polypyrrole for high-performance flexible supercapacitors. Polymers 10:135. https://doi.org/10.3390/polym10020135

Ji JY, Zhang LL, Ji HX, Li Y, Zhao X, Bai X, Fan XB, Zhang FB, Ruoff RS (2013) Nanoporous $Ni(OH)_2$ thin film on 3D ultrathin-graphite foam for asymmetric supercapacitor. ACS Nano 7:6237–6243. https://doi.org/10.1021/nn4021955

Liu YQ, Li C, Liu C, Chen Y, An K, Landskron K (2019) Probing the electrolyte infiltration behaviour of activated carbon supercapacitor electrodes by in situ neutron scattering using aqueous NaCl as electrolyte. Carbon 136:139–142. https://doi.org/10.1016/j.carbon.2018.04.072

Luo JL, Zheng Z, Kumamoto A, Unah WI, Yan SK, Ikuhara YH, Xiang X, Zu XT, Zhou WL (2018) PEDOT coated iron phosphide nanorod arrays as high-performance supercapacitor negative electrodes. Chem Commun 54:794–797. https://doi.org/10.1039/C7CC09163J

Ma YF, Chang HC, Zhang M, Chen YS (2015) Graphene-based materials for lithium-ion hybrid supercapacitors. Adv Mater 27:5296–5308. https://doi.org/10.1002/adma.201501622

Ma LB, Hu Y, Chen RP, Zhu GY, Chen T, Lv HL, Wang YR, Liang J, Liu HX, Yan CZ, Zhu HF, Tie ZX, Jin Z, Liu J (2016) Self-assembled ultrathin $NiCo_2S_4$ nanoflakes grown on Ni foam as high-performance flexible electrodes for hydrogen evolution reaction in alkaline solution. Nano Energy 24:139–147. https://doi.org/10.1016/j.nanoen.2016.04.024

Ma Y, Zhao DY, Chen YH, Huang J, Zhang ZX, Zhang XW, Zhang B (2019) A novel core-shell polyaniline/graphene oxide/copper nanocomposite for high performance and low-cost supercapacitors. Chem Pap 73:833–841. https://doi.org/10.1007/s11696-018-0556-x

Mao N, Chen WC, Meng J, Li YY, Zhang K, Qin XH, Zhang HN, Zhang CY, Qiu YP, Wang SR (2018) Enhanced electrochemical properties of hierarchically sheath-core aligned carbon nanofibers coated carbon fiber yarn electrode-based supercapacitor via polyaniline nanowire array modification. J Power Sources 399:406–413. https://doi.org/10.1016/j.jpowsour.2018.07.022

Mohit S, Kaushik N, Shaikh MM (2018) Emerging robust heterostructure of MoS_2–rGO for high-performance supercapacitors. ACS Appl Mater Interfaces 10:16588–16595. https://doi.org/10.1021/acsami.8b04540

Pai R, Kalra V (2018) High performance aqueous asymmetric supercapacitor based on iron oxide anode and cobalt oxide cathode. J Mater Res. https://doi.org/10.1557/jmr.2018.13

Pai R, Singh A, Simotwo S, Kalra V (2018) In situ grown iron oxides on carbon nanofibers as freestanding anodes in aqueous supercapacitors. Adv Eng Mater. https://doi.org/10.1002/adem.201701116

Pandit B, Karade SS, Sankapal BR (2017a) Hexagonal VS_2 anchored MWCNTs: first approach to design flexible solid-state symmetric supercapacitor device. ACS Appl Mater Interfaces 9:44880–44891. https://doi.org/10.1021/acsami.7b13908

Pandit B, Dubal DP, Romero PG, Kale BB, Sankapal BR (2017b) V_2O_5 encapsulated MWCNTs in 2D surface architecture: complete solid-state bendable highly stabilized energy efficient supercapacitor device. Sci Rep 7:43440. https://doi.org/10.1038/srep43430

Pazhamalai P, Krishnamoorthy K, Manoharan S, Kim SJ (2019) High energy symmetric supercapacitor based on mechanically delaminated few-layered MoS_2 sheets in organic electrolyte. J Alloy Compd 771:803–809. https://doi.org/10.1016/j.jallcom.2018.08.203

Sandhya V, Goban KP, Pratap K, Soon KJ, Andrews NG (2018) Solvothermal synthesis and electrochemical properties of phase pure pyrite FeS_2 for supercapacitor applications. Electrochim Acta 290:378–389. https://doi.org/10.1016/j.electacta.2018.09.027

Syed JA, Ma J, Zhu BG, Tang SC, Meng XK (2017) Hierarchical multicomponent electrode with interlaced $Ni(OH)_2$ nanoflakes wrapped zinc cobalt sulfide nanotube arrays for sustainable high-performance supercapacitors. Adv Energy Mater 7:1701228. https://doi.org/10.1002/aenm.201800106

Thakur AV, Lokhande BJ (2018) Source molarity affected surface morphological and electrochemical transitions in binder-free FeO(OH) flexible electrodes and fabrication of symmetric supercapacitive device. Chem Pap 72:1407–1415. https://doi.org/10.1007/s11696-018-0383-0

Thakur AV, Lokhande BJ (2019) Effect of precursor bath temperature on the morphology and electrochemical performance of SILAR-synthesized PPy:FeOOH hybrid flexible electrodes. Chem Pap 73:833–841. https://doi.org/10.1007/s11696-018-0644-y

Wang XH, Fang Y, Shi B, Huang FF, Rong F, Que RH (2018a) Three-dimensional $NiCo_2O_4$@$NiCo_2O_4$ core–shell nanocones arrays for high-performance supercapacitors. Chem Eng J 344:311–319. https://doi.org/10.1016/j.cej.2018.03.061

Wang ZY, Qin S, Seyedin S, Zhang JZ, Wang JT, Levitt A, Li N, Haines C, Robles RO, Lei WW, Gogotsi Y, Baughman RH, Razai JM (2018b) High-performance biscrolled MXene/carbon nanotube yarn supercapacitors. Small 14:180225. https://doi.org/10.1002/smll.201802225

Xing LL, Huang KJ, Cao SX, Pang H (2018) Chestnut shell-like $Li_4Ti_5O_{12}$ hollow spheres for high-performance aqueous asymmetric supercapacitors. Chem Eng J 332:253–259. https://doi.org/10.1016/j.cej.2017.09.084

Xiong T, Tan TL, Lu L, Lee WSV, Xue JM (2018) Harmonizing energy and power density toward 2.7 V asymmetric aqueous supercapacitor. Adv Energy Mater 8:1702630. https://doi.org/10.1002/aenm.201702630

Yang ZG, Liu NN, Dong S, Tian FS, Gao YP, Hou ZQ (2019) Supercapacitors based on free-standing reduced graphene oxides/carbon nanotubes hybrid films. SN Appl Sci 1:47. https://doi.org/10.1007/s42452-018-0059-y

Yu IZ, Lu BG, Xu Z (2014) Super long-life supercapacitors based on the construction of nanohoneycomb-like strongly coupled CoMoO4–3D graphene hybrid electrodes. Adv Mater 26:1044–1051. https://doi.org/10.1002/adma.201304148

Yuan WY, Cheng LF, Wu H, Zhang YN, Lv SL, Guo XH (2018) One-step synthesis of 2D-layered carbon wrapped transition metal nitrides from transition metal carbides (MXenes) for supercapacitors with ultrahigh cycling stability. Chem Commun 54:2755–2758. https://doi.org/10.1039/C7CC09017J

Zhang X, Zhu MC, Ouyang T, Chen Y, Zhu K, Ye K, Wang GL, Cheng K, Cao DX (2019) $NiFe_2O_4$ nanocubes anchored on reduced graphene oxide cryogel to achieve a 1.8 V flexible solid-state symmetric supercapacitor. Chem Eng J 360:171–179. https://doi.org/10.1016/j.cej.2018.11.206

Zhao P, Yao MQ, Ren HB, Wang Ni, Komameni S (2019) Nanocomposites of hierarchical ultrathin MnO_2 nanosheets/hollow carbon nanofibers for high-performance asymmetric supercapacitors. Appl Surf Sci 463:931–938. https://doi.org/10.1016/j.apsusc.2018.09.041

Zhi XM, Zhou HH (2018) Optimizing the preparation conditions of polypyrrole electrodes for enhanced electrochemical capacitive performances. Chem Pap 72:2513–2522. https://doi.org/10.1007/s11696-018-0473-z

Zhou QH, Wei T, Yue JM, Sheng LZ, Fan ZJ (2018) Polyaniline nanofibers confined into graphene oxide architecture for high-performance supercapacitors. Electrochim Acta 291:234–241. https://doi.org/10.1016/j.electacta.2018.08.104